Orientational Order and Instabilities in Suspensions of Self-Locomoting Rods

David Saintillan and Michael J. Shelley
Courant Institute of Mathematical Sciences, New York University, New York, New York 10012, USA
(Received 21 February 2007; published 30 July 2007)

The orientational order and dynamics in suspensions of self-locomoting slender rods are investigated numerically. In agreement with previous theoretical predictions, nematic suspensions of swimming particles are found to be unstable at long wavelengths as a result of hydrodynamic fluctuations. Nevertheless, a local nematic ordering is shown to persist over short length scales and to have a significant impact on the mean swimming speed. The consequences of the large-scale orientational disorder for particle dispersion are also discussed.

DOI: 10.1103/PhysRevLett.99.058102 PACS numbers: 87.18.Ed, 47.54.−r, 47.55.Kf, 87.18.Hf

Suspensions of swimming microorganisms are characterized by complex dynamics involving strong fluctuations and large-scale correlated motions. While these motions are in some cases driven by external fields, as in bioconvection or chemotaxis [1–3], they are also observed in bulk homogeneous suspensions where they result from the many-body hydrodynamic interactions between swimming particles [3–6]. These nonlinear dynamics are of fundamental interest, offering a new paradigm for pattern formation and self-organization in nonequilibrium systems. Their biological relevance is also clear, as these interactions impact effects such as mean particle transport, mixing, and diffusion, with possible consequences for nutrient uptake.

Interactions and pattern formation in active suspensions have been a long-standing problem of theoretical physics, e.g., [1,7]. Recently, Ramaswamy and co-workers [7–9] developed a continuum model based on a mean-field description of the stress exerted by the swimming particles on the suspending fluid. They investigated therein the stability of nematic suspensions and showed that in the low-Reynolds-number limit, nematic alignment is always unstable at long wavelengths, and should therefore lead to orientational disorder. While this instability may have been observed in experiments [3,5], a detailed study of orientational order in suspensions of swimming particles has yet to be performed.

In recent numerical simulations, Hernandez-Ortiz *et al.* [10] investigated suspensions of swimming particles modeled as rigid dumbbells exerting a force dipole on the fluid, which is the leading-order flow singularity induced by self-propelled particles. In agreement with experiments [5], they observed large-scale correlated regions in the disturbance flow created by the swimmers, with characteristic length scales greatly exceeding the particle dimensions. No detailed information on particle configurations inside these regions was reported.

In this Letter, we use numerical simulations to investigate aspects of orientation dynamics and microstructure in suspensions of self-locomoting rods at low Reynolds number. Our detailed model accounts for hydrodynamic interactions based on slender-body theory [11], and encompasses both biological [1] and nonbiological [12] locomotion mechanisms. We present the first clear demonstration of an orientational instability as predicted in Ref. [8]. In addition, we demonstrate that despite this long-wavelength instability an orientational order persists at short length scales, and we discuss its influence on the effective swimming speed of the particles.

We consider a suspension of N identical slender rodlike particles of length L, center-of-mass positions $\mathbf{x}$, and directors $\mathbf{n}$, which propel themselves by exerting an axisymmetric tangential shear stress on the fluid over a section of their body, while the remainder of their body is subject to the usual no-slip boundary condition. This surface shear stress, which is prescribed in our model, may represent the integrated effect of beating cilia on the surface of the microorganism [13], or the propagation of shape distortions along the particle surface [14]. The motion of a particle is modeled using local slender-body theory [11], adapted to the case of interest [15] as

$$\dot{\mathbf{x}} + s\dot{\mathbf{n}} + u_s(s)\mathbf{n} - \mathbf{u}'(s) = c(\mathbf{I} + \mathbf{nn}) \cdot [\mathbf{f}_{\|}(s) + \mathbf{f}_{\perp}(s)], \tag{1}$$

where s denotes a linear coordinate along the particle axis, $u_s(s)$ is a slip velocity on those parts of the body where the shear stress is prescribed, $\mathbf{u}'(s)$ is the disturbance velocity induced by the other particles in the suspension, $\mathbf{f}_{\|}(s)$ and $\mathbf{f}_{\perp}(s)$ denote the integrals over the azimuthal direction of the tangential and normal tractions on the particle surface, respectively, $c = \log(2/\epsilon)/4\pi\eta$ where $\epsilon \ll 1$ is the inverse aspect ratio, and η is the fluid viscosity. Where the swimming actuation occurs on the body, $\mathbf{f}_{\|}(s)$ is prescribed and $u_s(s)$ and $\mathbf{f}_{\perp}(s)$ have to be determined; where the no-slip boundary condition applies, $u_s(s) = 0$ and both $\mathbf{f}_{\|}(s)$ and $\mathbf{f}_{\perp}(s)$ are to be determined. Hydrodynamic interactions are captured through the disturbance velocity $\mathbf{u}'$, which is the fluid velocity induced by the force distributions $\mathbf{f}(s) = \mathbf{f}_{\|}(s) + \mathbf{f}_{\perp}(s)$ along the particles. It is obtained as

 © 2007 The American Physical Society

$$\mathbf{u}'(\mathbf{x}) = \frac{1}{8\pi\eta}\sum_i \int \mathbf{G}(\mathbf{x};\mathbf{x}_i + s_i\mathbf{n}_i)\cdot\mathbf{f}(s_i)ds_i, \quad (2)$$

where $\mathbf{G}(\mathbf{x};\mathbf{x}_0)$ is the Green function for Stokes flow in the geometry of interest. Equations (1) and (2), together with force and torque balances on all the rods, are solved in periodic boundary conditions for the force distributions and slip velocities using a spectral approximation of the disturbance velocity [15–18], together with a smooth particle-mesh Ewald algorithm to calculate hydrodynamic interactions [17]. The particle translational and angular velocities are then easily obtained from the zeroth and first moments of Eq. (1) with respect to s.

Two types of swimming microorganisms are considered: *pushers*, for which the shear stress actuation is near the particle tail, and *pullers*, for which it is near the head. We find that imposing a symmetric shear stress over the entire particle surface results in very weak interactions, a consequence of the absence of a net dipole in the force distribution exerted by the particle on the fluid. In the following, lengths, velocities, and times are scaled, respectively, by the particle length L, the isolated swimming speed U_0 (directly related to the integral of the imposed stress), and the characteristic time L/U_0. We define an effective volume fraction as $n(L/2)^3$ where n denotes the number density: this measure is of common use for suspensions of rodlike particles [19,20], where the transition from dilute to semidilute occurs at $n(L/2)^3 \approx 1$.

Motivated by the predictions of Refs. [7–9], we first consider the stability of uniform nematic suspensions of such swimmers in Fig. 1. The initial condition in Fig. 1(a) is a suspension aligned along the $\mathbf{z}$ direction with random center-of-mass distribution, with all the particles oriented to swim in the same direction (polar nematic suspension; see Ref. [8]); the case of an apolar suspension in which the swimming direction is arbitrary is qualitatively similar and addressed in Fig. 3(b). Very rapidly, the disturbance flow which results from the randomness in the particle arrangement causes the swimmers to rotate from their initial alignment [Fig. 1(b)]. The particles lose memory of their initial orientation [Fig. 1(c)], and at long times the orientation distribution is globally isotropic [Fig. 1(d)]. A typical flow field at long times is shown in Fig. 2(a), and is characterized by large-scale vortices and swirls in good agreement with previous observations [3,10].

The evolution of the orientation field is quantified by the polar and nematic order parameters: $S_1 = \langle \mathbf{n}\cdot\mathbf{z}\rangle$ and $S_2 = \frac{1}{2}\langle 3(\mathbf{n}\cdot\mathbf{z})^2 - 1\rangle$, shown as functions of time in Fig. 3. In the polar case of Fig. 1(a), $S_1 = S_2 = 1$ at $t = 0$. However, the suspension quickly becomes isotropic ($S_2 \to 0$), and loses its initial swimming direction ($S_1 \to 0$). In the apolar case [Fig. 3(b)], $S_1 = 0$ and $S_2 = 1$ at $t = 0$, and a similar destabilization occurs and the orientations also quickly evolve towards isotropy ($S_2 \to 0$). In all our simulations, the instability appears to occur at the scale of a few particle lengths, as is apparent in Fig. 1(b). Even at steady state, the microstructure of the suspension is clearly not random and isotropic at all length scales: as shown in Fig. 1(d), regions of correlated orientations persist over short scales even after the suspension has become isotropic on average. Strong density fluctuations are also present, and are found to be larger than in random suspensions as suggested in Ref. [8].

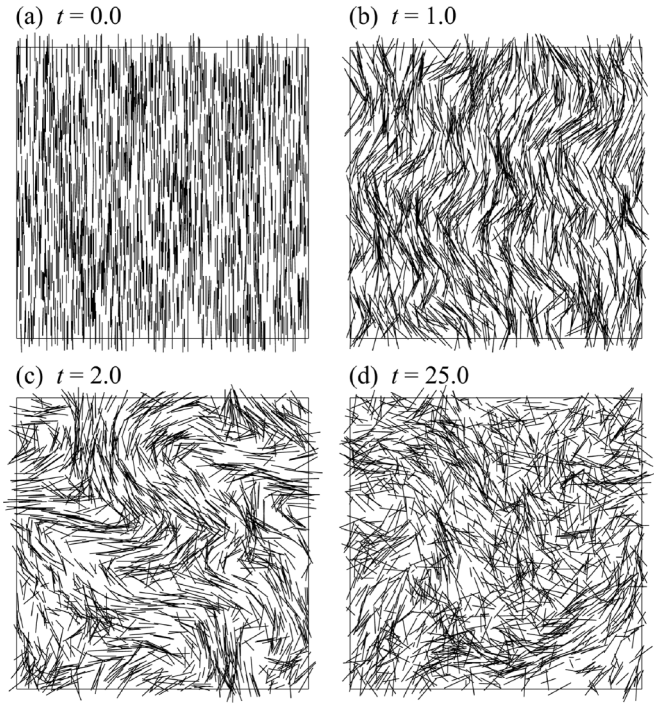

FIG. 1. Orientational instability in a polar nematic suspension of pushers, at an effective volume fraction of $n(L/2)^3 = 1.0$. The figure shows a region of dimensions $10 \times 10 \times 3$ (in units of particle length) containing 2500 particles at different stages of the instability (a)–(d).

To probe the local structure of the orientation field, we define the following polar and nematic pair correlation

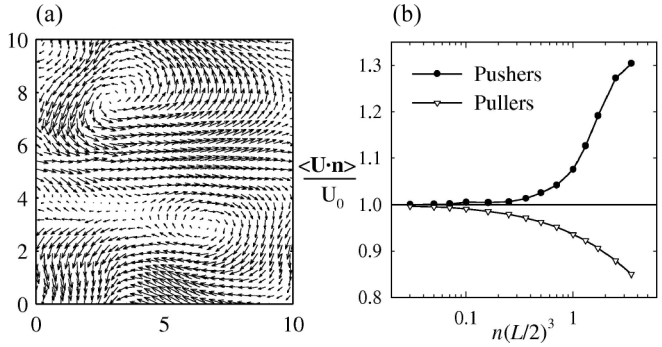

FIG. 2. (a) Typical disturbance flow field at long times in a plane cross section in the simulation of Fig. 1. (b) Mean swimming speed $\langle \mathbf{U}\cdot\mathbf{n}\rangle$ along the particle director $\mathbf{n}$, normalized by the isolated swimming speed U_0, as a function of the effective volume fraction $n(L/2)^3$.

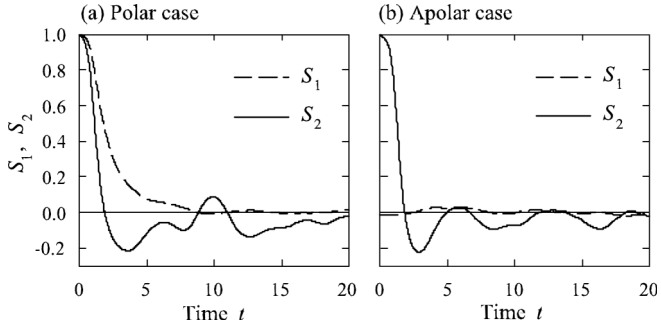

FIG. 3. Time evolution of the polar and nematic order parameters S_1 and S_2 during the instability of Fig. 1 for (a) polar and (b) apolar initial orientation distributions, in suspensions of pushers.

functions for the director $\mathbf{n}$:

$$C_1(r) = \frac{\langle \sum_{i\neq j} (\mathbf{n}_i \cdot \mathbf{n}_j)\delta(|\mathbf{x}_i - \mathbf{x}_j| - r)\rangle}{\langle \sum_{i\neq j} \delta(|\mathbf{x}_i - \mathbf{x}_j| - r)\rangle},$$
$$C_2(r) = \frac{\langle \sum_{i\neq j} \frac{1}{2}[3(\mathbf{n}_i \cdot \mathbf{n}_j)^2 - 1]\delta(|\mathbf{x}_i - \mathbf{x}_j| - r)\rangle}{\langle \sum_{i\neq j} \delta(|\mathbf{x}_i - \mathbf{x}_j| - r)\rangle}, \quad (3)$$

where δ is the three-dimensional Dirac delta function. Figure 4(a) shows $C_1(r)$ and $C_2(r)$ for both pushers and pullers at $n(L/2)^2 = 1.0$. For pushers, $C_1(r)$, $C_2(r) > 0$ for small r; i.e., nearby pushers have a high probability of being nearly parallel with the same swimming direction (polar nematic ordering); at larger values of r the orientations decorrelate, and a weak anticorrelation is sometimes observed. In suspensions of pullers, however, $C_1(r)$, $C_2(r) < 0$ for small r; i.e., nearby pullers are likely to be misaligned and swimming in opposite directions. In both cases, a local ordering exists at short length scales as a result of the fluid disturbance flow [Fig. 2(a)]. The existence of distinct polarities for the alignment of pushers and pullers is, however, surprising, and arises from the specific features of hydrodynamic interactions between these two types of particles.

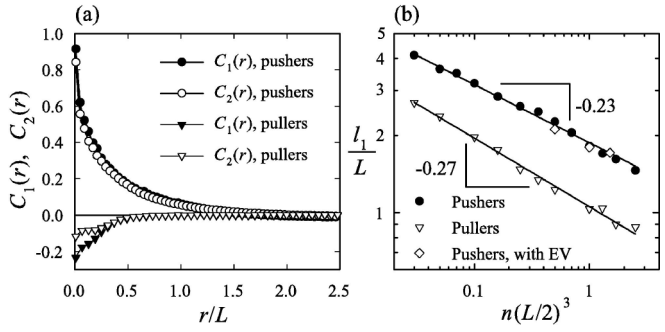

FIG. 4. (a) Polar and nematic pair correlation functions $C_1(r)$ and $C_2(r)$ at steady state in suspensions of pushers and pullers at a volume fraction of $n(L/2)^3 = 1.0$. (b) Correlation length l_1, or first zero of the polar pair correlation function $C_1(r)$ in (a), as a function of volume fraction for both pushers and pullers, with and without excluded volume (EV).

The position of the first zero of $C_1(r)$, $r = l_1$, estimates the spatial extent of these nematically ordered regions and is shown in Fig. 4(b) for both pushers and pullers as a function of volume fraction. It is found to decrease with volume fraction, and the dependence is well captured by a power law of exponent ≈ -0.25. Remarkably, in very dilute suspensions the radius of the correlated regions can exceed ≈ 3 or 4 particle lengths. While the majority of the simulations presented here neglected excluded volume (EV), a few simulations were performed in which steric interactions were included by means of a short-range repulsive potential: as shown in Fig. 4(b), the effect of excluded volume on the correlation length is negligible up to at least $n(L/2)^3 \approx 1.5$, and the effect on particle diffusivities is also very weak (Fig. 5). At higher volume

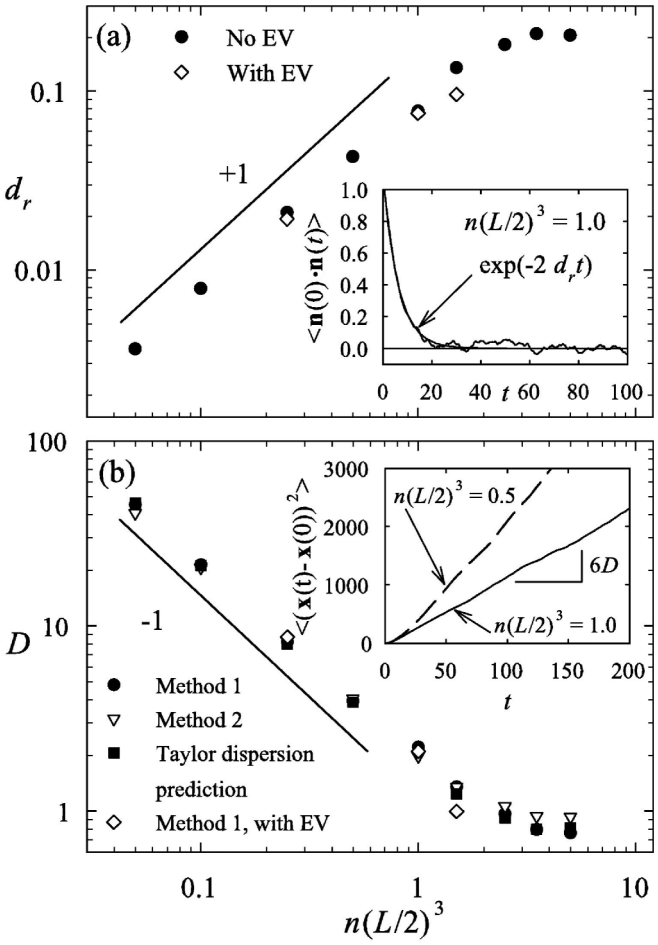

FIG. 5. (a) Orientational dispersion coefficient d_r as a function of volume fraction in suspensions of pushers, determined from the time autocorrelation function of the director $\mathbf{n}$ (inset), with and without EV. (b) Center-of-mass dispersion coefficient D in suspensions of pushers. D was obtained independently using the integral of the velocity autocorrelation function (method 1) and using mean-square displacements (method 2 and inset), and is compared to the Taylor dispersion prediction $D = U_0^2/6d_r$.

fractions, larger departures may be expected (see Ref. [21] for a study focusing on excluded volume without hydrodynamic interactions).

Figure 2(b) shows the effect of the local nematic ordering on the mean swimming speed $\langle \mathbf{U} \cdot \mathbf{n} \rangle$ of the particles along their directors, normalized by the swimming speed of an isolated swimmer. This effect is significant at moderate and high concentrations, where pushers are found to swim faster than in the isolated case, whereas pullers swim more slowly. This observation suggests a mechanical advantage to tail swimming actuation, which results in more effective transport in concentrated suspensions.

Because the particles interact and effectively travel through a chaotic flow, their orientations decorrelate in time, leading to hydrodynamic dispersion. The effective orientational dispersion coefficient d_r associated with this process can be determined from the characteristic time scale for relaxation of particle orientations [19]: $\langle \mathbf{n}(0)\mathbf{n}(t) \rangle = \frac{1}{3}\mathbf{I} \exp(-2d_r t)$. This coefficient is plotted in Fig. 5(a) as a function of $n(L/2)^3$ in suspensions of pushers. At low $n(L/2)^3$, d_r grows linearly with volume fraction, suggesting that the dispersion results mainly from pair interactions. The growth slows down beyond $n(L/2)^3 \approx 1$, which may be related to the screening of hydrodynamic interactions.

The corresponding center-of-mass dispersion coefficient D is shown in Fig. 5(b). D was determined independently as the integral of the time autocorrelation function of the particle velocities: $D = \frac{1}{3}\int_0^\infty \langle \dot{\mathbf{x}}(0) \cdot \dot{\mathbf{x}}(t) \rangle dt$, and as the long-time growth rate of the mean-square displacements in the suspension: $D = \lim_{t\to\infty} \frac{1}{6}\frac{d}{dt}\langle (\mathbf{x}(t) - \mathbf{x}(0))^2 \rangle$, with good agreement between the two methods. As in Ref. [10], the dispersion coefficient D is found to decrease with concentration at low values of $n(L/2)^3$, followed by a plateau at higher $n(L/2)^3$. The initial decrease suggests that the main mechanism for center-of-mass dispersion is not direct particle interactions, as these would cause an increase of D with concentration. Instead, center-of-mass dispersion is here a consequence of the orientational dispersion which randomizes the swimming direction of the particles, resulting in a random walk over long times. This process may be modeled using Brenner's generalized Taylor dispersion theory [22,23], which yields the prediction $D = U_0^2/6d_r$ for the dispersion coefficient, in excellent agreement with the simulation data at low and moderate concentrations.

While only the case of bulk homogeneous suspensions was presented here, simulations in thin liquid films were also performed to reproduce the experimental conditions of Ref. [5]. Similar orientational dynamics and correlated motions were also observed, along with a strong concentration of the particles near the interface, in qualitative agreement with previous simulations in confined geometries [10]. Dynamics in an external field such as a chemical gradient can also be addressed within the framework of our model: in that case mean particle transport will be governed by the balance between chemotaxis and hydrodynamic fluctuations, and a stabilization of particle orientations may be expected in very strong gradients.

We thank R. Goldstein and D. Cai for useful conversations. This work is supported by NSF Grant No. DMS-0412203 and DOE Grant No. DE-FG02-88ER25053.

[1] T. J. Pedley and J. O. Kessler, Annu. Rev. Fluid Mech. **24**, 313 (1992).
[2] N. A. Hill and T. J. Pedley, Fluid Dyn. Res. **37**, 1 (2005).
[3] C. Dombrowski *et al.*, Phys. Rev. Lett. **93**, 098103 (2004).
[4] N. H. Mendelson *et al.*, J. Bacteriol. **181**, 600 (1999).
[5] X.-L. Wu and A. Libchaber, Phys. Rev. Lett. **84**, 3017 (2000).
[6] G. V. Soni *et al.*, Biophys. J. **84**, 2634 (2003).
[7] J. Toner, Y. Tu, and S. Ramaswamy, Ann. Phys. (N.Y.) **318**, 170 (2005).
[8] R. A. Simha and S. Ramaswamy, Phys. Rev. Lett. **89**, 058101 (2002).
[9] S. Ramaswamy and R. A. Simha, Solid State Commun. **139**, 617 (2006).
[10] J. P. Hernandez-Ortiz, C. G. Stoltz, and M. D. Graham, Phys. Rev. Lett. **95**, 204501 (2005).
[11] G. K. Batchelor, J. Fluid Mech. **44**, 419 (1970).
[12] W. F. Paxton *et al.*, J. Am. Chem. Soc. **126**, 13 424 (2004).
[13] C. Brennen and H. Winet, Annu. Rev. Fluid Mech. **9**, 339 (1977).
[14] H. A. Stone and A. D. T. Samuel, Phys. Rev. Lett. **77**, 4102 (1996).
[15] D. Saintillan and M. J. Shelley (to be published).
[16] J. E. Butler and E. S. G. Shaqfeh, J. Fluid Mech. **468**, 205 (2002).
[17] D. Saintillan, E. Darve, and E. S. G. Shaqfeh, Phys. Fluids **17**, 033301 (2005).
[18] A.-K. Tornberg and K. Gustavsson, J. Comput. Phys. **215**, 172 (2006).
[19] M. Doi and S. F. Edwards, *The Theory of Polymer Dynamics* (Oxford University Press, Oxford, 1986).
[20] R. Blanc, in *Mobile Particulate Systems*, edited by E. Guazzelli and L. Oger (Kluwer, Dordrecht, 1995).
[21] N. Sambelashvili, A. W. C. Lau, and D. Cai, Phys. Lett. A **360**, 507 (2007).
[22] H. Brenner, PCH. Physicochem. Hydrodyn. **1**, 91 (1980).
[23] H. Brenner, J. Colloid Interface Sci. **71**, 189 (1979).